Multifunctional Ruthenium(II) Polypyridine Complex-Based Core–Shell Magnetic Silica Nanocomposites: Magnetism, Luminescence, and Electrochemiluminescence

Mei-Jin Li,[†] Zuofeng Chen,[†] Vivian Wing-Wah Yam,[†,‡,*] and Yanbing Zu[†,*]

[†]Department of Chemistry, The University of Hong Kong, Pokfulam Road, Hong Kong, P.R. China, and [‡]State Key Laboratory of Supramolecular Structure and Materials, Jilin University, Changchun, P.R. China

ABSTRACT Multifunctional nanoparticles (NPs) that consist of silica-coated magnetic cores and luminescent ruthenium(II) polypyridine complexes have been prepared. These multifunctional nanocomposites were shown to exhibit superparamagnetic behavior, high emission intensity, and electrochemiluminescence. An intense low-oxidation-potential electrochemiluminescence signal was observed by attachment of these functional NPs onto a fluorosurfactant-modified gold (Au_m) electrode *via* application of an external magnetic field.

KEYWORDS: luminescence · magnetic nanoparticle · core-shell structure · silica-coated · electrochemiluminescence · ruthenium(II) polypyridine complex · multifunctional

Magnetic nanoparticles (NPs) have attracted significant interest in the past years and have been widely studied for microbiology, biochemistry, bioanalytical chemistry, and biomedicine applications such as MRI contrast enhancement,[1] magnetic immobilization,[2] bioelectrocatalysis,[3] and drug targeting.[4,5] In particular, much attention have been paid to the investigation of polymer- or SiO_2-coated magnetic nanoparticles as a result of their superparamagnetic properties and biocompatibility.[6–11] In many applications, silica serves as an attractive candidate to encapsulate these magnetic nanoparticles because of its stability, biocompatibility, easy functionalization, and low cytotoxicity.[12–16] The combination of magnetic and luminescence properties into a single micro- or nanocomposite system would be very useful in the biomedical and biopharmaceutical fields.[17,18] Some reports have focused on the synthesis and investigation of bifunctional nanomaterials such as core-shell nanocomposites.[19] In most cases, organic dyes or metal complexes were immobilized on the silica layer, which suffers from severe problems of leaching and photobleaching. In other cases, quantum dots (QDs) were used as luminescent labels, although QDs are less chemically stable and potentially toxic and may show fluorescence intermittence.[20,21] Recently, $[Ru(bpy)_3]^{2+}$-encapsulated silica nanoparticles were extensively applied in bioanalysis and biodetection as a result of their good stability and high luminescence quantum yield.[22–24] During the course of our study, there were also recent reports on the electrochemiluminescence (ECL) of $[Ru(bpy)_3]^{2+}$-encapsulated silica nanoparticles, which served as tri-*n*-propylamine (TPrA) or polyamine sensors.[25–27] In those studies, $[Ru(bpy)_3]^{2+}$ could be directly oxidized on the electrode surface to produce an ECL signal. The diameters of most silica-coated magnetic NPs and dye-encapsulated silica NPs prepared and studied are larger than 50 nm, and there has been a growing interest in the synthesis of smaller-sized functional magnetic NPs as this would facilitate their applications in biomedical sciences because of their higher surface area and the possibility of larger dye loading. From our recent interest in the synthesis of functional nanoparticles[28–32] and our long-standing interest in luminescent metal-based materials,[33–36] here we report the synthesis and investigation of multifunctional core-shell magnetic silica nanocomposites, with the Fe_3O_4 core coated with a silica shell, to which luminescent ruthenium(II) complexes were covalently attached and further encapsulated with an additional layer of silica shell. The magnetic,

*Address correspondence to wwyam@hku.hk, ybzu@hku.hk.

Received for review February 29, 2008 and accepted April 14, 2008.

Published online May 7, 2008.
10.1021/nn800123w CCC: $40.75

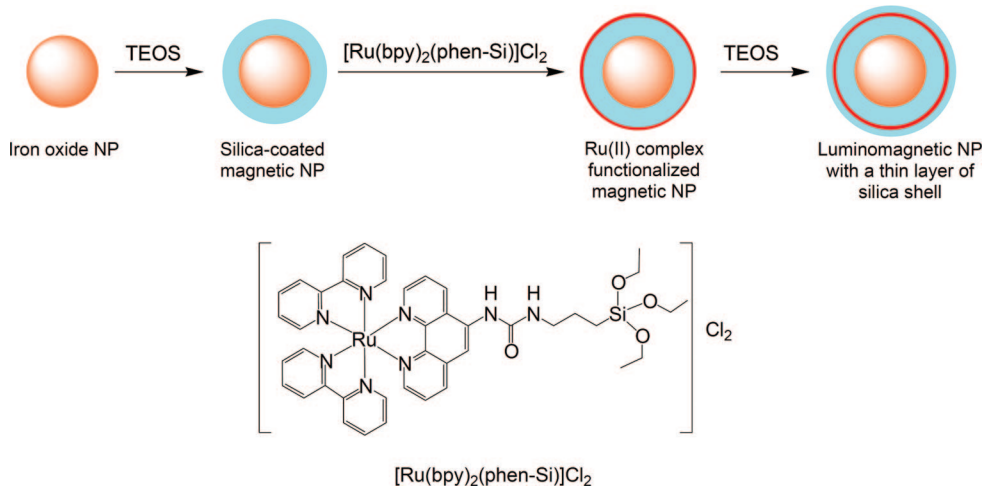

Scheme 1. Synthetic scheme for the multifunctional magnetic nanoparticles and the chemical structure of $[Ru(bpy)_2(phen\text{-}Si)]Cl_2$.

luminescent, and ECL behavior of these nanocomposites has also been studied.

RESULTS AND DISCUSSION

Synthesis and Characterization of Luminomagnetic NPs. The synthetic procedure for functionalized luminomagnetic NPs and the chemical structure of the ruthenium(II) complex are shown in Scheme 1. The Fe_3O_4 nanoparticles were synthesized according to the literature method.[37] The silica-coated magnetic nanoparticles were prepared in a reverse microemulsion medium by modification of a reported method.[12] The method was simple, and the thickness of the silica shell was readily tuned by control of the amount of tetraethyl orthosilicate (TEOS) used and the reaction time. The first layer of silica coating serves to isolate the ruthenium(II) polypyridine luminophore from the magnetic core to avoid luminescence quenching and to provide silanol groups for the covalent immobilization of the ruthenium(II) complexes. The thin layer of silica shell at the outermost surface of the nanoparticles serves to avoid the direct contact of the ruthenium(II) complexes with the electrode surface to prevent their direct oxidation on the electrode surface. The luminomagnetic NPs are rather monodisperse and spherical in shape, and their TEM images are depicted in Figure 1. The $Fe_3O_4@SiO_2$ core-shell structure of the nanocomposites is obvious, as revealed from the TEM images, with a diameter of 18 ± 3 nm and a silica shell thickness of *ca.* 7 nm. Since the monolayer of the ruthenium(II) complex is too thin to be observed by TEM, it is difficult to differentiate the inner silica layer and the outer protective silica layer from the TEM image. Because of the aggregation of iron oxide nanoparticles prior to or during the coating process, there could be more than one magnetic nanoparticle trapped in some of these nanocomposites, which may be advantageous when manipulating the core-shell nanoparticles with an external magnetic field. Energy-dispersive X-ray (EDX) analysis also indicates the presence of Fe, Si, and Ru (Supporting Information, Figure S1).

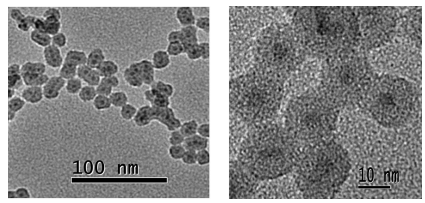

Figure 1. TEM images of luminomagnetic nanoparticles at different magnifications.

The magnetic properties of the silica-coated Fe_3O_4 magnetic nanoparticles and luminomagnetic nanoparticles were characterized by vibrating sample magnetometer at room temperature. As shown in Figure 2, both of them exhibit negligible coercivity and remanence, typical of superparamagnetic materials, and their saturation magnetization was 2.0 and 1.3 emu/g, respectively. Compared with other silica-coated magnetic nanoparticles, the lower saturation magnetization of these functional nanoparticles could be attributed to the presence of the outer shell of silica. Interestingly, the nanocomposites when dispersed in solution were also inductive to the external magnetic field. When a handheld magnet was placed close to the glass vial, the nanocomposites were attracted to the magnet very

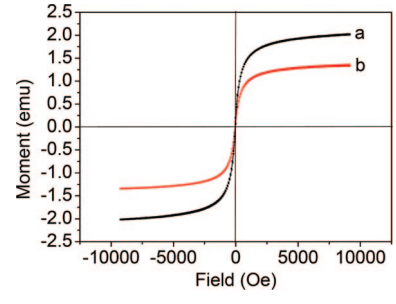

Figure 2. Magnetization curves of (a) silica-coated iron oxide nanoparticles and (b) luminomagnetic nanoparticles at room temperature.

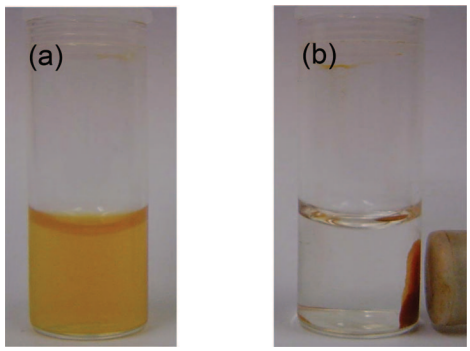

Figure 3. Photographs of the luminomagnetic nanoparticles dispersed in aqueous solution (a) without and (b) with an external magnetic field.

quickly and accumulated near it within several minutes, leaving the bulk solution clear and transparent (Figure 3). The clear transparent liquid shows neither absorption nor emission. After removal of the external magnet and upon vigorous shaking, the nanocomposites could be rapidly redispersed again, demonstrating the magnetic separation characteristics of the multifunctional nanoparticles.

Electronic Absorption and Emission Properties of the Luminomagnetic NPs. The UV−vis absorption spectra of a suspension of silica-coated magnetic NPs, luminomagnetic NPs, and the ruthenium(II) complex in aqueous solution are shown in Figure 4a. Compared to the spectra of the silica-coated iron oxide nanoparticles and the ruthenium(II) complex in aqueous solution, the UV−vis absorption bands of the luminomagnetic NPs at *ca.* 285 and 400−500 nm are assigned as the intraligand (IL) and the metal-to-ligand charge transfer (MLCT) transitions of the ruthenium(II) polypyridine

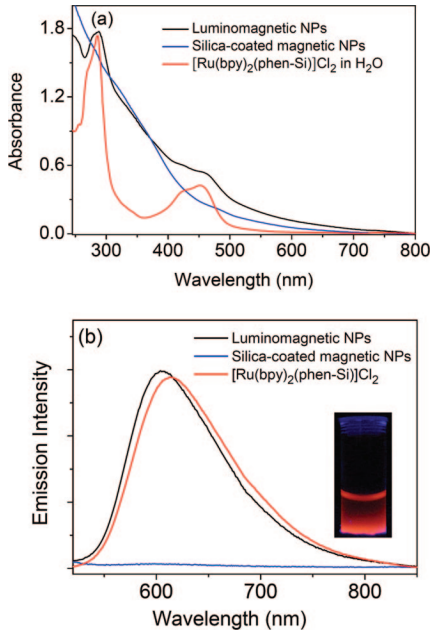

Figure 4. (a) UV−vis absorption and (b) emission spectra of NPs and $[Ru(bpy)_2(phen\text{-}Si)]Cl_2$ in H_2O. The inset shows the image of luminomagnetic NPs under UV irradiation.

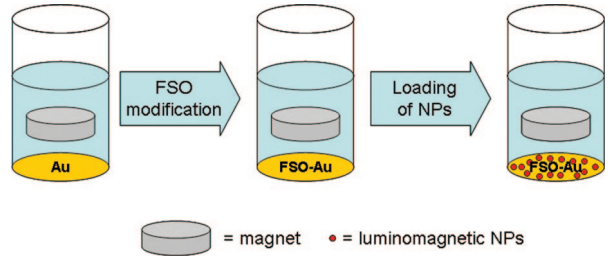

Scheme 2. Schematic representation of the electrode modification process (not in scale).

complex, respectively, confirming the successful immobilization of the ruthenium(II) complexes to the magnetic nanocomposites.

The emission spectra of the functionalized nanoparticles and the ruthenium(II) complex in aqueous solution are shown in Figure 4b. The silica-coated iron oxide nanoparticles were found to be nonemissive upon light excitation. On the contrary, the luminomagnetic NPs gave rise to a strong emission originating from the characteristic emission of the ruthenium(II) polypyridine complex, with the well-dispersed aqueous solution of multifunctional nanoparticles showing a strong red-orange emission (Figure 4b inset). Compared to the ruthenium(II) complex in aqueous solution, the multifunctional nanoparticles showed a slight blue shift of *ca.* 10 nm in the emission wavelength, similar to that observed in other ruthenium(II) polypyridine immobilized silica nanoparticles.[38]

Electrochemistry of the Luminomagnetic NPs. The gold electrode was modified with the use of a magnet as illustrated schematically in Scheme 2 to attach the luminomagnetic NPs onto the gold electrode surface. As a magnet was used to collect the luminomagnetic NPs onto the electrode surface, the immobilization of the NPs was simple, effective, and reversible. The luminomagnetic NPs were accumulated on the Au_m electrode both in the absence (NPs-Au_m) and in the presence of an adsorbed FSO layer (NPs-FSO-Au_m). The electrochemistry of the luminomagnetic NPs on the bare Au_m electrode was studied. As shown in Figure 5, the cyclic voltammogram (CV) of the luminomagnetic NPs-coated Au_m electrode exhibited characteristic redox waves similar to those of the bare Au_m electrode, except that

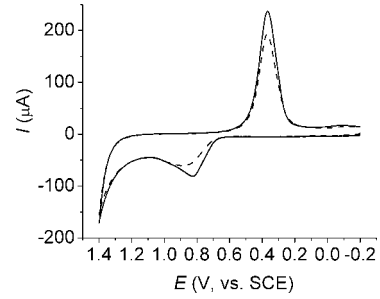

Figure 5. Cyclic voltammograms obtained at the Au_m electrode (solid line) and the NPs-Au_m electrode (dashed line). Solution, 0.15 M PBS (pH 7.5). Scan rate, 100 mV/s.

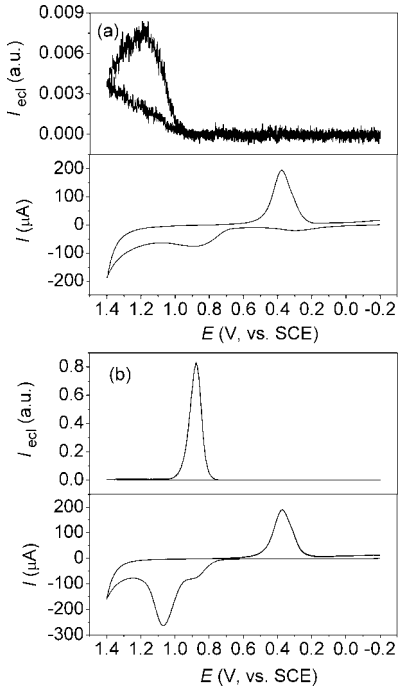

Figure 6. CV-ECL curves obtained at (a) the NPs-Au_m electrode and (b) the NPs-FSO-Au_m electrode. Solution, 0.15 M PBS (pH 7.5) containing 1 mM TPrA. Scan rate, 100 mV/s.

the active surface area was slightly smaller. Interestingly, the redox wave corresponding to the $Ru^{3+/2+}$ couple was not observed, indicating that most of the $[Ru(bpy)_2(phen\text{-}Si)]^{2+}$ species were out of the electron tunneling distance (~1−2 nm) from the electrode and could not be oxidized directly. This observation lent further evidence to support the presence of an outer silica protective layer surrounding the NPs. It is interesting to note that with other immobilization approaches, such as a Nafion-coated electrode, the incorporated $[Ru(bpy)_3]^{2+}$ usually undergoes a diffusion process, and distinct redox waves corresponding to the $Ru^{3+/2+}$ couple could be observed.[39–41]

ECL Responses from the Luminomagnetic NPs. The ECL of $[Ru(bpy)_2(phen\text{-}Si)]^{2+}$-tagged NPs was examined using TPrA as the coreactant. Figure 6 shows the CV-ECL curves obtained at the NPs-Au_m and NPs-FSO-Au_m electrodes with 1 mM TPrA. In the absence of the fluorosurfactant (FSO) species, the CV and ECL profiles at the luminomagnetic NPs-loaded Au_m electrode were similar to that of $[Ru(bpy)_3]^{2+}$ in aqueous solution reported previously.[42] TPrA oxidation occurred in the potential region where the electrode surface oxides started to grow, and the oxidation current overlapped completely with that of the gold surface. The ECL peak at *ca.* +1.15 V was produced *via* the conventional emission routes. However, in the presence of FSO, the initial growth of the electrode surface oxides was significantly suppressed, and facile TPrA oxidation was achieved, showing an anodic wave below +1.0 V (note that the large anodic peak at *ca.* +1.05 V might result mainly from the desorption of the surfactant species and the rapid oxidation of the electrode surface[43]). A low-oxidation-potential (LOP) ECL signal appeared along with the TPrA oxidation. When compared with the ECL peak at +1.15 V on the NPs-Au_m electrode, a 110-fold enhanced ECL signal has been achieved at a much less positive potential (*ca.* +0.88 V) when the electrode was pretreated with FSO. The strong enhancement of the LOP ECL signal was striking. As mentioned earlier, most of the $[Ru(bpy)_2(phen\text{-}Si)]^{2+}$ species on the NPs could not be oxidized directly, and therefore the ECL *via* the conventional routes which required the oxidation of $[Ru(bpy)_2(phen\text{-}Si)]^{2+}$ would be greatly limited. On the contrary, the immobilized $[Ru(bpy)_2(phen\text{-}Si)]^{2+}$ species could still contribute to the intense LOP ECL response because their oxidation was not required in this route.

LOP ECL Intensity as a Function of the Loading Mass of the Luminomagnetic NPs. According to the LOP ECL mechanism, the direct oxidation of TPrA plays an important role. It has been found that the loading of the luminomagnetic NPs on the electrode would influence TPrA oxidation as well as the LOP ECL intensity, as shown in Figure 7. With an increase in the loading of NPs on the electrode, the TPrA oxidation current was found to decrease gradually because of a decrease in the area of the gold electrode surface due to the blocking by the NPs. In contrast, the LOP ECL intensity was found to increase rapidly as the luminomagnetic NPs were immobilized and reached a maximum at ~0.3 mg loading, after which the emission intensity started to drop. The decrease of the LOP ECL intensity at high NP loading might be due to the smaller TPrA oxidation current. In addition, the accumulated NPs would also physically block the emission light from reaching the photomultiplier tube detector, leading to the measured decrease in the ECL intensity.[44]

Amine Sensing and Detection. The ECL of $[Ru(bpy)_3]^{2+}$ and its derivatives has been used extensively in chemical analysis for the sensitive detection of numerous an-

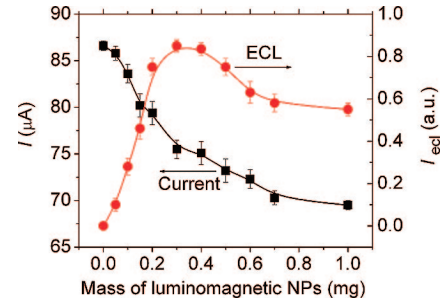

Figure 7. TPrA oxidation current (■) and corresponding LOP ECL intensity (●) versus the loading mass of the luminomagnetic NPs on the FSO-Au_m electrode. Solution, 0.15 M PBS (pH 7.5) containing 1 mM TPrA. Scan rate, 100 mV/s.

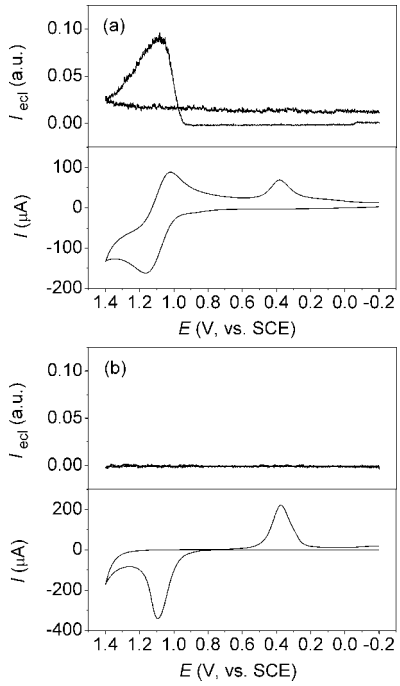

Figure 8. CV-ECL curves obtained at (a) the $[Ru(bpy)_3]^{2+}$-NF-Au_m electrode and (b) the NPs-FSO-Au_m electrode. Solution, 0.15 M PBS (pH 7.5). Scan rate, 100 mV/s.

alytes such as alkylamines, oxalate, amino acids, and NADH.[45,46] These analytes were detected as the coreactants with $[Ru(bpy)_3]^{2+}$ species in solution, and continuous delivery of $[Ru(bpy)_3]^{2+}$ species into the reaction zone was required, which would greatly increase the experimental cost and complexity. To overcome this limitation, $[Ru(bpy)_3]^{2+}$ species are usually immobilized on the electrode surface, of which the incorporation of $[Ru(bpy)_3]^{2+}$ species in the cation exchange polymer Nafion has been the most popular method.[39,40,47–49] Furthermore, to achieve high sensitivity, $[Ru(bpy)_3]^{2+}$ (or its derivatives) is usually preconcentrated on the electrode surface, and the ECL is produced predominantly *via* the catalytic route, which would usually lead to large background ECL signals.[39,49] In the absence of any coreactants, as shown in Figure 8a, when the electrode potential was scanned positively beyond *ca.* +1.0 V, the Nafion-immobilized $[Ru(bpy)_3]^{2+}$ was oxidized, producing an intense ECL signal. The ECL signal observed might be due to the reaction of $[Ru(bpy)_3]^{3+}$, the electro-oxidization product of $[Ru(bpy)_3]^{2+}$, with hydroxide ion in solution, as reported previously.[50] However, when the luminomagnetic NPs were employed, the background ECL signal was found to be essentially suppressed, as shown in Figure 8b. Since most of the immobilized $[Ru(bpy)_2(phen\text{-}Si)]^{2+}$ did not have any direct contact with the electrode and could not be oxidized, the ECL background arising from the reaction of $[Ru(bpy)_2(phen\text{-}Si)]^{3+}$ with hydroxide was effectively reduced, especially in the potential region where the LOP ECL was produced.

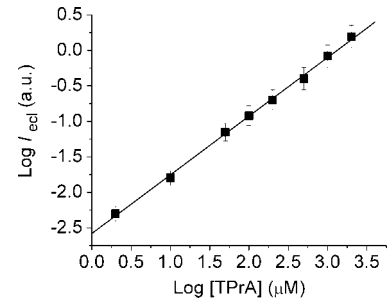

Figure 9. Calibration plot for the detection of TPrA with a luminomagnetic NPs(0.3 mg)-loaded FSO-Au_m electrode. Solution, 0.15 M PBS (pH 7.5) containing different concentrations of TPrA. Scan rate, 100 mV/s.

Figure 9 illustrates a typical log−log calibration plot for the detection of TPrA at the NPs(0.3 mg)-FSO-Au_m electrode. The linear concentration range was found to extend from 2 μM to 2 mM ($R^2 = 0.998$) with a detection limit of 1 μM ($S/N = 3$). Better detection sensitivity could probably be achieved by using a flow-cell system. The main advantage of the present method lies in the fact that no oxidation of the ruthenium(II) complex is required in the light-generating step and, therefore, the background ECL signal is small.

To date, several methods, including Langmuir−Blodgett technique,[51,52] self-assembly technique[53,54] or the incorporation of $[Ru(bpy)_3]^{2+}$ within the cation-exchange polymer Nafion, have been developed to immobilized $[Ru(bpy)_3]^{2+}$ species on an electrode surface.[39,40,47,48] A common problem in such systems is the low stability of the modified electrodes. For example, Langmuir−Blodgett films were easily washed from the electrode with chloroform, [51] self-assembled films were unstable during the potential scan;[53] and Nafion-based modified electrodes usually suffered from the leaching of the $[Ru(bpy)_3]^{2+}$ species from the electrode surface or the partition of $[Ru(bpy)_3]^{2+}$ into the more hydrophobic regions of Nafion.[39] In our method reported here, since ruthenium(II) complex species are covalently attached onto the NPs that are magnetically attached to the electrode, leaching of the emitting species can be avoided. Furthermore, it is envisaged that this kind of multifunctional magnetic nanoparticles has great potential applications as luminescent biolabels and in bioseparation.

CONCLUSION

Multifunctional ruthenium(II) polypyridine complex-based core-shell magnetic Fe_3O_4@SiO_2 nanocomposites have been successfully prepared. Leach-free properties and protection of the ruthenium(II) complexes from direct contact with external surfaces such as an electrode surface were achieved. Interestingly, the redox wave corresponding to the $Ru^{3+/2+}$ couple was not observed, indicating that most of the ruthenium(II) species were out of the electron tunneling distance (*ca.* 1−2 nm) from the electrode, while an intense LOP ECL signal was achieved in the presence of fluorosurfactant species

with TPrA as coreactant. The sensing of TPrA was also studied and the main advantage of the method involves an efficient suppression of the background ECL signal as the oxidation of the ruthenium(II) complexes is not required in the light-generating step. The much lower potentials required in the LOP ECL route may also be extended for future DNA diagnostic work, as it has been well-documented that oligonucleotide sequences may undergo irreversible oxidative damage at potentials above +1 V.

MATERIALS AND METHODS

Chemicals. 5-Amino-1,10-phenanthroline, 3-(triethoxysilyl)propyl isocyanate, triton X-100, tris(2,2′-bipyridyl)ruthenium(II) dichloride hexahydrate ($Ru(bpy)_3Cl_2 \cdot 6H_2O$, min 98%), tri-*n*-propylamine (TPrA, 98%), Zonyl FSO-100 ($F(CF_2CF_2)_{1-7}CH_2CH_2O(CH_2CH_2O)_{0-15}H$), and Nafion perfluorinated ion-exchange resin (5 wt % solution in a mixture of lower aliphatic alcohols and 15−20% water) were purchased from Sigma-Aldrich. Other chemicals were of analytical grade and were used as received. *cis*-$[Ru(bpy)_2Cl_2] \cdot xH_2O$ were synthesized according to the literature procedure.[55] All aqueous solutions were prepared with deionized water (Milli-Q, Millipore). The pH of the phosphate buffer solution (PBS) was adjusted with concentrated NaOH or phosphoric acid.

Physical Measurments and Instrumentation. ^{1}H NMR spectra were recorded on a Bruker DPX-300 or Bruker DPX-400 Fourier Transform NMR spectrometer with chemical shifts reported relative to tetramethylsilane. Positive-ion FAB mass spectra were recorded on a Finnigan MAT95 mass spectrometer. Elemental analysis of the complexes was performed on a Carlo Erba 1106 elemental analyzer at the Institute of Chemistry of the Chinese Academy of Sciences in Beijing. Electronic absorption spectra were recorded on a Hewlett-Packard 8452A diode array spectrophotometer. Steady state emission spectra at room temperature were recorded on a Spex Fluorolog-2 model F 111 fluorescence spectrophotometer. TEM images were recorded on a Tecnai 20 (Philips) transmission electron microscope with an accelerating voltage of 200 kV at the Electron Microscope Unit (EMU) of The University of Hong Kong. Cyclic voltammetry (CV) was performed with the model 600A electrochemical workstation (CH Instruments, Austin, TX). The three-electrode system consisted of a working electrode, a coiled Pt wire counter electrode, and a saturated calomel reference electrode (SCE) separated from the working cell by a salt bridge. The ECL signal was measured with a photomultiplier tube (PMT, Hamamatsu R928) installed under the electrochemical cell. A voltage of −800 V was supplied to the PMT with a Sciencetech PMH-02 instrument (Sciencetech Inc., Hamilton, Ontario, Canada).

Synthesis of Ligand (phen-Si). The ligand was prepared by modification of literature procedures.[56,57] 5-Amino-1,10-phenanthroline (0.16 g, 8.2 mmol) was dissolved in $CHCl_3$ (15 mL), and 3-(triethoxysilyl)propyl isocyanate (0.22 mL, 9.0 mmol) was added to the solution. The mixture was then reduced to a volume of ~1 mL, and the mixture was stirred under N_2 at 80 °C for overnight. The crude product was purified by column chromatography on silica gel with $CHCl_3$/MeOH (50:1 v/v) as the eluent to give the product as a pale yellow solid. Yield: 0.20 g, 55%. Positive FAB-MS: *m/z* 443. ^{1}H NMR (300 MHz, $CDCl_3$): δ 8.95 (d, *J* = 3.6 Hz, 1H, phen), 8.76 (d, *J* = 3.6 Hz, 1H, phen), 8.68 (s, broad, 1H, NH), 8.31 (d, *J* = 8.1 Hz, 1H, phen), 8.17 (s, 1H, phen), 8.10 (d, *J* = 8.1 Hz, 1H, phen), 7.51 (dd, *J* = 8.1 Hz, 3.6 Hz, 1H, phen), 7.12(dd, *J* = 8.1 Hz, 3.6 Hz, 1H, phen), 6.52 (s, broad, 1H, NH), 3.72 (m, 6H, $SiOCH_2$), 3.30 (m, 2H, CH_2), 1.64 (m, 2H, CH_2), 1.14 (t, *J* = 7.0 Hz, 9H, CH_3), 0.60 (t, *J* = 8.4 Hz, 2H, CH_2Si). The chemical shifts of protons on NH and phenanthroline showed changes at different concentrations due to the effect of intermolecular hydrogen bonding.

Synthesis of Ruthenium(II) Complex ($[Ru(bpy)_2(phen\text{-}Si)]Cl_2$). This was prepared by modification of a literature method for $[Ru(bpy)_2(phen)]^{2+}$.[58] To a solution of *cis*-$[Ru(bpy)_2Cl_2] \cdot xH_2O$ (50 mg, 0.096 mmol) in absolute ethanol (50 mL) was added phen-Si (53 mg, 0.12 mmol), and the mixture was heated to reflux under N_2 for 5 h, during which the purple-black solution turned red-orange. After removal of the solvent under reduced pressure, the residue was recrystallized from $CHCl_3$/diethyl ether to give the desired complex as a red solid. Yield: 52 mg, 58%. ^{1}H NMR (400 MHz, $CDCl_3$): δ 10.72 (s, 1H, NH), 10.06 (d, *J* = 8.6 Hz, 1H, pyridyl H), 9.04 (d, *J* = 9.1 Hz, 1H, pyridyl H), 8.98 (d, *J* = 9.1 Hz, 1H, pyridyl H), 8.92 (s, 1H, phen), 8.77 (m, 2H, pyridyl H), 8.28 (d, *J* = 8.2 Hz, 1H, pyridyl H), 8.16 (m, 2H, pyridyl H), 8.06 (m, 2H, pyridyl H), 7.90 (m, 3H, pyridyl H), 7.83 (d, *J* = 5.5 Hz, 1H, pyridyl H), 7.76 (m, 2H, pyridyl H), 7.59 (m, 2H, pyridyl H), 7.47(d, *J* = 5.4 Hz, 1H, pyridyl H), 7.40 (d, *J* = 5.4 Hz, 1H, pyridyl H), 7.29 (m, 2H, pyridyl H), 3.82 (m, 6H, OCH_2), 3.34 (m, 2H, CH_2), 1.78 (m, 2H,CH_2), 1.22 (t, *J* = 7.0 Hz, 9H, CH_3), 0.75 (t, *J* = 8.4 Hz, 2H, CH_2Si). Positive FAB-MS: *m/z* 891 ($[M - Cl]^+$), 855 ($[M - 2Cl]^+$). Anal. Found: C, 52.66; H, 4.89; N, 11.51. Calcd. for $C_{42}H_{46}Cl_2N_8O_4RuSi \cdot 1.5H_2O$: C, 52.88; H, 5.18; N, 11.75.

Synthesis of Core-Shell (Silica-Coated) Magnetic Nanoparticles. Fe_3O_4 nanoparticles were synthesized by literature method.[37] The core-shell magnetic nanoparticles were prepared by modification of a reported procedure.[12] Typically, triton X-100 (1.30 g, 2 mmol) was dissolved in cyclohexane (20 mL) by sonication, and then Fe_3O_4 in cyclohexane (0.2 mL, 5 mg/mL) was added. The mixture was sonicated for 5 min, and ammonium hydroxide solution (140 μL, 28%) was added with sonication to form a clear brown microemulsion. Tetraethyl orthosilicate (TEOS, 80 μL) was then added, and the reaction was continued for 16 h at room temperature with vigorous stirring. The nanoparticles were precipitated upon addition of ethanol and collected by centrifugation, washed with ethanol three times, and then redispersed in ethanol (10 mL).

Synthesis of Multifunctional Magnetic Nanoparticles. Covalent attachment of the ruthenium(II) complex to the silica shell was achieved by modification of a literature method.[59] A solution of $[Ru(bpy)_2(phen\text{-}Si)]Cl_2$ (2 mg) dissolved in ethanol (10 mL) was added to the ethanol-dispersed silica-coated magnetic nanoparticles (10 mL) with stirring, and the mixture was heated to reflux overnight. After the reaction, the ruthenium(II) complex-modified magnetic nanoparticles were obtained by centrifugation, washed with ethanol several times to remove the excess ruthenium(II) complex, and then redispersed in ethanol (10 mL). An ethanolic solution (2 mL) of TEOS (20 μL) was added to a mixture of ammonium hydroxide solution (15 μL, 28%), H_2O (10 μL), and the previously obtained ruthenium(II) complex-modified magnetic nanoparticle in ethanol (10 mL) with stirring. The hydrolysis and condensation of TEOS onto the surface of the nanoparticles were completed at room temperature within 10 h. The luminomagnetic nanoparticles were collected by centrifugation, washed with ethanol three times, and redispersed in ethanol or water depending on the experimental condition.

Preparation of Modified Electrodes. The magnetic Au electrode (Au_m, 0.163 cm^2) was prepared by incorporating a magnet (diameter 2 mm, height 1.5 mm) into the body of the electrode holder. Prior to the experiments, the Au_m electrode was wet polished with 0.05 μm Al_2O_3 powders to obtain a mirror surface, followed by sonication in distilled water for 10 s, and was subjected to repeated scanning in a wide potential range in 0.1 M H_2SO_4 solution until reproducible voltammograms were obtained. The FSO-modified Au_m electrode (FSO-Au_m) was prepared by dipping the pretreated Au_m electrode into a 1 wt % FSO aqueous solution for 5 min, followed by a thorough rinsing with distilled water. The FSO-Au_m electrode was then placed in the aqueous dispersion of luminomagnetic NPs (~1 mL) to collect most of the luminomagnetic NPs within ~20 min. The mass of the loaded NPs on the resulting electrode (NPs-FSO-Au_m) could be controlled by varying the amount of the NPs in the dispersion.

The Nafion-coated Au_m electrode (NF-Au_m) was obtained by carefully spreading 6 μL of 2 wt % Nafion solution (diluted with methanol) on the cleaned Au_m surface, followed by drying at room temperature for 0.5 h. Better stability was obtained if the Nafion was heated for 1 min in a hot water bath (100 °C) prior to application to the electrode.[39] The Nafion-coated electrode was then immersed for 15 min in 0.15 M PBS (pH 7.5) containing 1 mM $[Ru(bpy)_3]Cl_2$, rinsed thoroughly with distilled water, and transferred to the electrochemical cell. The electrode ($[Ru(bpy)_3]^{2+}$-NF-Au_m) prepared in this manner acquired a deep orange color, demonstrating the large amount of $[Ru(bpy)_3]^{2+}$ incorporated into the polymer.

Solution pH was adjusted to 7.5 to obtain an intense LOP ECL signal.[60] To eliminate the influence of oxygen,[61] solutions were deaerated by bubbling high purity (99.995%) N_2, and a constant flow of N_2 was maintained over the solution during the measurements. All potentials reported are with reference to the SCE. All experiments were performed at 20 ± 1 °C. Reported values for CV-ECL are based on the average of at least three repeated experiments.

Acknowledgment. V.W.-W.Y. acknowledges receipt of the Distinguished Research Achievement Award from The University of Hong Kong. The authors also acknowledge support from the National Natural Science Foundation of China and the Research Grants Council of Hong Kong Joint Research Scheme (NSFC-RGC Project No. N_HKU 737/06) and the Research Grants Council of Hong Kong Special Administration Region, PR China (RGC CERG Project No. HKU 7059/05P). Discussions with Dr. B. Li and Dr. D.-B. Yu at the early stage of this project are acknowledged.

Supporting Information Available: Energy-dispersive X-ray (EDX) analysis of multifunctional magnetic nanoparticles and the LOP ECL mechanism of the $[Ru(bpy)_3]^{2+}$/TPrA system. This material is available free of charge *via* the Internet at http://pubs.acs.org.

REFERENCES AND NOTES

1. Tanaka, T.; Matsunaga, T. Fully Automated Chemiluminescence Immunoassay of Insulin using Antibody-Protein A-Bacterial Magnetic Particle Complexes. *Anal. Chem.* **2000**, *72*, 3518–3522.
2. Wuang, S. C.; Neoh, K. G.; Kang, E. T.; Pack, D. W.; Leckband, D. E. Heparinized Magnetic Nanoparticles: In-Vitro Assessment for Biomedical Applications. *Adv. Funct. Mater.* **2006**, *16*, 1723–1730.
3. Riskin, M.; Basnar, B.; Huang, Y.; Willner, I. Magnetoswitchable Charge Transport and Bioelectrocatalysis Using Maghemite-Au Core-Shell Nanoparticle/Polyaniline Composites. *Adv. Mater.* **2007**, *19*, 2691–2695.
4. Levy, L.; Sahoo, Y.; Kim, K.-S.; Bergey, E. J.; Prasad, P. N. Nanochemistry: Synthesis and Characterization of Multifunctional Nanoclinics for Biological Applications. *Chem. Mater.* **2002**, *14*, 3715–3721.
5. Nasongkla, N.; Bey, E.; Ren, J.; Ai, H.; Khemtong, C.; Guthi, J. S.; Chin, S. F.; Sherry, A. D.; Boothman, D. A.; Gao, J. Multifunctional Polymeric Micelles as Cancer-Targeted, MRI-Ultrasensitive Drug Delivery Systems. *Nano Lett.* **2006**, *6*, 2427–2430.
6. Yoon, T. J.; Kim, J. S.; Kim, B. G.; Yu, K. N.; Cho, M. H.; Lee, J. K. Multifunctional Nanoparticles Possessing a "Magnetic Motor Effect" for Drug or Gene Delivery. *Angew. Chem., Int. Ed.* **2005**, *44*, 1068–1071.
7. Euliss, L. E.; Grancharov, S. G.; O'Brien, S.; Deming, T. J.; Stucky, G. D.; Murray, C. B.; Held, G. A. Cooperative Assembly of Magnetic Nanoparticles and Block Copolypeptides in Aqueous Media. *Nano Lett.* **2003**, *3*, 1489–1493.
8. Yi, D. K.; Selvan, S. T.; Lee, S. S.; Papaefthymiou, G. C.; Kundaliya, D.; Ying, J. Y. Silica-Coated Nanocomposites of Magnetic Nanoparticles and Quantum Dots. *J. Am. Chem. Soc.* **2005**, *127*, 4990–4991.
9. Lu, Y.; Yin, Y.; Mayers, B. T.; Xia, Y. Modifying the Surface Properties of Superparamagnetic Iron Oxide Nanoparticles Through a Sol-Gel Approach. *Nano Lett.* **2002**, *2*, 183–186.
10. Vestal, C. R.; Zhang, Z. J. Synthesis and Magnetic Characterization of Mn and Co Spinel Ferrite-Silica Nanoparticles with Tunable Magnetic Core. *Nano Lett.* **2003**, *3*, 1739–1743.
11. Yi, D. K.; Lee, S. S.; Ying, J. Y. Synthesis and Applications of Magnetic Nanocomposite Catalysts. *Chem. Mater.* **2006**, *18*, 2459–2461.
12. Yi, D. K.; Lee, S. S.; Papaefthymiou, G. C.; Ying, J. Y. Nanoparticle Architectures Templated by SiO_2/Fe_2O_3 Nanocomposites. *Chem. Mater.* **2006**, *18*, 614–619.
13. Liz-Marzan, L. M.; Giersig, M.; Mulvaney, P. Homogeneous Silica Coating of Vitreophobic Colloids. *Chem. Commun.* **1996**, 731–732.
14. Tartaj, P.; Serna, C. J. Synthesis of Monodisperse Superparamagnetic Fe/Silica Nanospherical Composites. *J. Am. Chem. Soc.* **2003**, *125*, 15754–15755.
15. Tartaj, P.; Gonzalez-Carreno, T.; Serna, C. J. Single-Step Nanoengineering of Silica Coated Maghemite Hollow Spheres with Tunable Magnetic Properties. *Adv. Mater.* **2001**, *13*, 1620–1624.
16. Ennas, G.; Musinu, A.; Piccaluga, G.; Zadda, D.; Gatteschi, D.; Sangregorio, C.; Stanger, J. L.; Concas, G.; Spano, G. Characterization of Iron Oxide Nanoparticles in an Fe_2O_3-SiO_2 Composite Prepared by a Sol-Gel Method. *Chem. Mater.* **1998**, *10*, 495–502.
17. Kim, H.; Achermann, M.; Balet, L. P.; Hollingsworth, J. A.; Klimov, V. I. Synthesis and Characterization of Co/CdSe Core/Shell Nanocomposites: Bifunctional Magnetic-Optical Nanocrystals. *J. Am. Chem. Soc.* **2005**, *127*, 544–546.
18. Zheng, Q.; Ohulchanskyy, T. Y.; Sahoo, Y.; Prasad, P. N. Water-Dispersible Polymeric Structure Co-encapsulating a Novel Hexa-*peri*-hexabenzocoronene Core Containing Chromophore with Enhanced Two-Photon Absorption and Magnetic Nanoparticles for Magnetically Guide Two-Photon Cellular Imaging. *J. Phys. Chem. C* **2007**, *111*, 16846–16851.
19. Yoon, T.-J.; Yu, K. N.; Kim, E.; Kim, J. S.; Kim, B. G.; Yun, S.-H.; Sohn, B.-H.; Cho, M.-H.; Lee, J.-K.; Park, S. B. Specific Targeting, Cell Sorting, and Bioimaging with Smart Magnetic Silica Core-Shell Nanomaterials. *Small* **2006**, *2*, 209–215.
20. Uyeda, H. T.; Medintz, I. L.; Jaiswal, J. K.; Simon, S. M.; Mattoussi, H. Synthesis of Compact Multidentate Ligands To Prepare Stable Hydrophilic Quantum Dot Fluorophores. *J. Am. Chem. Soc.* **2005**, *127*, 3870–3878.
21. Hohng, S.; Ha, T. Near-Complete Suppression of Quantum Dot Blinking in Ambient Conditions. *J. Am. Chem. Soc.* **2004**, *126*, 1324–1325.
22. Herr, J. K.; Smith, J. E.; Medley, C. D.; Shangguan, D.; Tan, W. Aptamer-Conjugated Nanoparticles for Selective Collection and Detection of Cancer Cells. *Anal. Chem.* **2006**, *78*, 2918–2919.
23. Smith, J. E.; Medley, C. D.; Tang, Z.; Shangguan, D.; Lofton, C.; Tan, W. Aptamer-Conjugated Nanoparticles for the Collection and Detection of Multiple Cancer Cells. *Anal. Chem.* **2007**, *79*, 3075–3082.
24. Rossi, L. M.; Shi, L.; Quina, F. H.; Rosenzweig, Z. Stöber Synthesis of Monodispersed Luminescent Silica Nanoparticles for Bioanalytical Assays. *Langmuir* **2005**, *21*, 4277–4280.
25. Zhang, L. H.; Dong, S. J. Electrogenerated Chemiluminescence Sensors using $Ru(bpy)_3^{2+}$ Doped in Silica Nanoparticles. *Anal. Chem.* **2006**, *78*, 5119–5123.
26. Zhang, L. H.; Dong, S. J. Electrogenerated Chemiluminescence Sensing Platform using $Ru(bpy)_3^{2+}$ Doped Silica Nanoparticles and Carbon Nanotubes. *Electrochem. Commun.* **2006**, *8*, 1687–1691.
27. Zhang, L. H.; Liu, B. F.; Dong, S. J. Bifunctional Nanostructure of Magnetic Core Luminescent Shell and Its Application as Solid-State Electrochemiluminescence Sensor Material. *J. Phys. Chem. B* **2007**, *111*, 10448–10452.

28. Yu, D.; Yam, V. W.-W. Controlled Synthesis of Monodisperse Silver Nanocubes in Water. *J. Am. Chem. Soc.* **2004**, *126*, 13200–13201.
29. Yu, D.; Yam, V. W.-W. Hydrothermal-Induced Assembly of Colloidal Silver Spheres into Various Nanoparticles on the Basis of HTAB-Modified Silver Mirror Reaction. *J. Phys. Chem. B* **2005**, *109*, 5497–5503.
30. Li, Q.; Yam, V. W.-W. High-Yield Synthesis of Selenium Nanowires in Water at Room Temperature. *Chem. Commun.* **2006**, 1006–1008.
31. Li, Q.; Yam, V. W.-W. Redox Luminescence Switch Based on Energy Transfer in $CePO_4$:Tb^{3+} Nanowires. *Angew. Chem., Int. Ed.* **2007**, *46*, 3486–3489.
32. Lu, C.; Zu, Y.; Yam, V. W.-W. Specific Postcolumn Detection Method for HPLC Assay of Homocysteine Based on Aggregation of Fluorosurfactant-Capped Gold Nanoparticles. *Anal. Chem.* **2007**, *79*, 666–672.
33. Yam, V. W.-W. Molecular Design of Transition Metal Alkynyl Complexes as Building Blocks for Luminescent Metal-Based Materials: Structural and Photophysical Aspects. *Acc. Chem. Res.* **2002**, *35*, 555–563.
34. Yam, V. W.-W.; Wong, K. M.-C.; Zhu, N. Solvent-Induced Aggregation through Metal $\cdots$ Metal/$\pi \cdots \pi$ Interactions: Large Solvatochromism of Luminescent Organoplatinum(II) Terpyridyl Complexes. *J. Am. Chem. Soc.* **2002**, *124*, 6506–6507.
35. Wong, K. M.-C.; Hung, L. L.; Lam, W. H.; Zhu, N.; Yam, V. W.-W. A Class of Luminescent Cyclometalated Alkynylgold(III) Complexes: Synthesis, Characterization, and Electrochemical, Photophysical, and Computational Studies of [Au(C^N^C)(C$\equiv$C$-$R)] (C^N^C = κ^3C,N,C Bis-cyclometalated 2,6-Diphenylpyridyl). *J. Am. Chem. Soc.* **2007**, *129*, 4350–4365.
36. Li, M.-J.; Chu, B. W.-K.; Yam, V. W.-W. Synthesis, Characterization, Spectroscopic, and Electroluminescence Properties of a Solvatochromic Azacrown-Containing Cyanoruthenate(II): Potential Applications in Separation and Indirect Photometric Detection of Cations and Amino Acids in HPLC. *Chem. Eur. J.* **2006**, *12*, 3528–3537.
37. Sun, S.; Zeng, H. Size-Controlled Synthesis of Magnetite Nanoparticles. *J. Am. Chem. Soc.* **2002**, *124*, 8204–8205.
38. Bagwe, R. P.; Yang, C.; Hilliard, L. R.; Tan, W. Optimization of Dye-Doped Silica Nanoparticles Prepared using a Reverse Microemulsion Method. *Langmuir* **2004**, *20*, 8336–8342.
39. Downey, T. M.; Nieman, T. A. Chemiluminescence Detection using Regenerable Tris(2,2′-bipyridyl)ruthenium(II) Immobilized in Nafion. *Anal. Chem.* **1992**, *64*, 261–268.
40. Rubinstein, I.; Bard, A. J. Polymer Films on Electrodes. 4. Nafion-Coated Electrodes and Electrogenerated Chemiluminescence of Surface-Attached Tris(2,2′-bipyridine)ruthenium(II). *J. Am. Chem. Soc.* **1980**, *102*, 6641–6642.
41. Rubinstein, I.; Bard, A. J. Polymer Films on Electrodes. 5. Electrochemistry and Chemiluminescence at Nafion-Coated Electrodes. *J. Am. Chem. Soc.* **1981**, *103*, 5007–5013.
42. Zu, Y.; Bard, A. J. Electrogenerated Chemiluminescence. 66. The Role of Direct Coreactant Oxidation in the Ruthenium Tris(2,2′)bipyridyl/Tripropylamine System and the Effect of Halide Ions on the Emission Intensity. *Anal. Chem.* **2000**, *72*, 3223–3232.
43. Li, F.; Zu, Y. Effect of Nonionic Fluorosurfactant on the Electrogenerated Chemi- luminescence of the Tris(2,2′-bipyridine)ruthenium(II)/Tri-*n*-propylamine System: Lower Oxidation Potential and Higher Emission Intensity. *Anal. Chem.* **2004**, *76*, 1768–1762.
44. Komori, K.; Takada, K.; Hatozaki, O.; Oyama, N. Electrochemiluminescence of Ru(II) Complexes Immobilized on a Magnetic Microbead Surface: Distribution of Magnetic Microbeads on the Electrode Surface and Effect of Azide Ion. *Langmuir* **2007**, *23*, 6446–6452.
45. Knight, A. W. A Review of Recent Trends in Analytical Applications of Electrogenerated Chemiluminescence. *Trends Anal. Chem.* **1999**, *18*, 47–62.
46. Gerardi, R. D.; Barnett, N. W.; Lewis, S. W. Analytical Applications of Tris(2,2′ -bipyridyl)ruthenium(III) as a Chemiluminescent Reagent. *Anal. Chim. Acta* **1999**, *378*, 1–41.
47. Lee, W. Y.; Nieman, T. A. Evaluation of Use of Tris(2,2′-bipyridyl)ruthenium(III) as a Chemiluminescent Reagent for Quantitation in Flowing Streams. *Anal. Chem.* **1995**, *67*, 1789–1796.
48. Martin, A. F.; Nieman, T. A. Glucose Quantitation using an Immobilized Glucose Dehydrogenase Enzyme Reactor and a Tris(2,2′-bipyridyl) Ruthenium(II) Chemiluminescent Sensor. *Anal. Chim. Acta* **1993**, *281*, 475–481.
49. Khramov, A. N.; Collinson, M. M. Electrogenerated Chemiluminescence of Tris(2,2′-bipyridyl)ruthenium(II) Ion-Exchanged in Nafion-Silica Composite Films. *Anal. Chem.* **2000**, *72*, 2943–2948.
50. Hercules, D. M.; Lytle, F. E. Chemiluminescence from Reduction Reactions. *J. Am. Chem. Soc.* **1966**, *88*, 4745–4746.
51. Zhang, X.; Bard, A. J. Electrogenerated Chemiluminescent Emission from an Organized (L-B) Monolayer of a Tris(2,2′-bipyridine)ruthenium(II)-Based Surfactant on Semiconductor and Metal Electrodes. *J. Phys. Chem.* **1988**, *92*, 5566–5569.
52. Miller, C. J.; McCord, P.; Bard, A. J. Study of Langmuir Monolayers of Ruthenium Complexes and their Aggregation by Electrogenerated Chemiluminescence. *Langmuir* **1991**, *7*, 2781–2787.
53. Sato, Y.; Uosaki, K. Electrochemical and Electrogenerated Chemiluminescence Properties of Tris(2,2′-bipyridine)ruthenium(II)-Tridecanethiol Derivative on ITO and Gold Electrodes. *J. Electroanal. Chem.* **1995**, *384*, 57–66.
54. Obeng, Y. S.; Bard, A. J. Electrogenerated Chemiluminescence. 53. Electrochemistry and Emission from Adsorbed Monolayers of a Tris(bipyridyl)ruthenium(II)-Based Surfactant on Gold and Tin Oxide Electrodes. *Langmuir* **1991**, *7*, 195–201.
55. Sullivan, B. P.; Salmon, D. J.; Meyer, T. J. Mixed Phosphine 2,2′-Bipyridine Complexes of Ruthenium. *Inorg. Chem.* **1978**, *17*, 3334–3341.
56. Kloster, G. M.; Taylor, C. M.; Watton, S. P. Effects of Multiple Covalent Attachments on Immobilized Iron(II)-1,10-phenanthroline Complexes in Silica Sol-Gels. *Inorg. Chem.* **1999**, *38*, 3954–3955.
57. Kloster, G. M.; Watton, S. P. Oxidation of Immobilized Iron(II)-1,10-phenanthroline Complexes by Cerium(IV): A Probe into the Site Accessibility of Metal Complexes Covalently Attached to Silica Sol-Gels. *Inorg. Chim. Acta* **2000**, *297*, 156–161.
58. Crosby, G. A.; Elfring, W. H. Excited States of Mixed Ligand Chelates of Ruthenium(II) and Rhodium(III). *J. Phy. Chem.* **1976**, *80*, 2206–2211.
59. Yu, S. Y.; Zhang, H. J.; Yu, J. B.; Wang, C.; Sun, L. N.; Shi, W. D. Bifunctional Magnetic-Optical Nanocomposites: Grafting Lanthanide Complex onto Core-Shell Magnetic Silica Nanoarchitecture. *Langmuir* **2007**, *23*, 7836–7840.
60. Zu, Y.; Li, F. Characterization of the Low-Oxidation-Potential Electrogenerated Chemiluminescence of Tris(2,2′-bipyridine)ruthenium(II) with Tri-*n*-propylamine as Coreactant. *Anal. Chim. Acta* **2005**, *550*, 47–52.
61. Zheng, H.; Zu, Y. Emission of Tris(2,2′-bipyridine)ruthenium(II) by Coreactant Electrogenerated Chemiluminescence: From O_2-Insensitive to Highly O_2-Sensitive. *J. Phys. Chem. B* **2005**, *109*, 12049–12053.